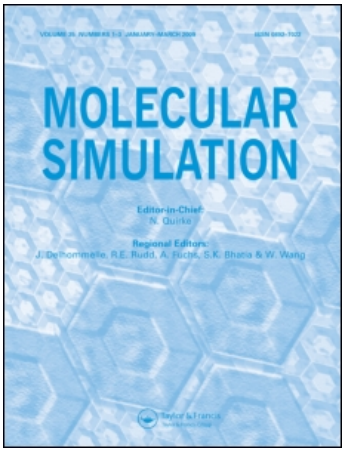

Molecular Simulation
Publication details, including instructions for authors and subscription information:
http://www.informaworld.com/smpp/title~content=t713644482

Engineering nanocrystals of silicon

John C. L. Cornish[a]; Eman Mohamed[a]; Reem Abdelaal[a]
[a] Physics and Energy studies, Murdoch University, Murdoch WA 6150, Australia

To cite this Article Cornish, John C. L. , Mohamed, Eman and Abdelaal, Reem(2005) 'Engineering nanocrystals of silicon', Molecular Simulation, 31: 6, 405 — 410
To link to this Article: DOI: 10.1080/08927020412331332695
URL: http://dx.doi.org/10.1080/08927020412331332695

Molecular Simulation, Vol. 31, Nos. 6–7, 15 May – 30 May 2005, 405–410

Engineering nanocrystals of silicon

JOHN C.L. CORNISH, EMAN MOHAMED and REEM ABDELAAL

Physics and Energy studies, Murdoch University, Murdoch WA 6150, Australia

(Received September 2004; in final form September 2004)

In this paper we describe the production of nanocrystals of silicon embedded in an amorphous silicon matrix. These were then modified by partially removing the amorphous phase. The band gap that defines the optoelectronic properties of silicon changes with crystallite size. Silicon nanocrystals exhibit a significant blue shift in the band gap with decreasing size. The contribution of the nanocrystals to the properties of the amorphous silicon matrix depends on their size, shape, orientation, distribution and volume fraction. These are properties that we are investigating and modifying. Such engineering of the optical and electronic properties could lead to new and improved optoelectronic devices. Thin films of silicon ranging from fully amorphous to polycrystalline have been deposited from pure silane by the Hot Wire method. The effect of deposition conditions: filament temperature, substrate temperature, silane flow rate, pressure, and time have been investigated. The conditions under which isolated nanocrystals embedded in an amorphous matrix form have been mapped. Selected films have been anisotropically etched to enhance the nanocrystalline features. The films have been investigated using UV–visible spectroscopy, Raman Spectroscopy, Fourier transform infra-red spectroscopy, transmission electron microscopy and selected area electron diffraction.

Keywords: Silicon; Thin films; Anisotropic etching; Crystalline fraction

PACS Numbers: 78.67.Bf Nanocrystals and nanoparticles

1. Introduction

Silicon is one of the world's most plentiful elements and has found many uses in the electronics industry. Its unique properties recommend it as a material to play a substantial role in new devices based on nanotechnological principles. In this paper we describe the production of nanocrystals of silicon embedded in an amorphous silicon matrix. These were then modified by preferentially removing the amorphous phase.

A regular array of nanocrystals could form a photonic crystal structure with useful properties. Our work is directed towards achieving this. A regular array is more difficult to achieve than a random array, but there are several approaches that will be followed in future work.

Small crystals of semiconductors, in the range of 2–10 nm, are termed protocrystals, nanocrystals or, quantum dots, larger crystals 10–20 nm are microcrystals [1]. Small crystallites have different optical and electronic properties from the bulk material. As more atoms are added to the nanocrystal particles and as they grow in size, the properties of these crystallites eventually approach the bulk values. In particular, the band gap that defines the optical and electronic properties of these materials changes with size. As a result, silicon nanocrystals exhibit a significant blue shift in optical properties from the bulk infra-red band gap energy to the visible range [2]. The band gap of the nanocrystals varies with the size of the nanoparticle. The contribution of the nanocrystals to the amorphous silicon film, depends on their size, shape, orientation, distribution and volume fraction. These are properties that we are investigating and trying to control.

2. Experimental

Thin films of silicon ranging from fully amorphous to polycrystalline have been deposited by the Hot Wire method, in which pure silane is passed over a hot tungsten filament and the resulting ions and radicals interact with the growing surface to form a thin film [3]. The deposition was carried out in a purpose built chamber with an airlock and transport system [4]. The effect of deposition conditions: filament temperature, substrate temperature, flow rate, gas pressure, and deposition time have been investigated enabling the conditions under which isolated nanocrystals embedded in an amorphous matrix are formed to be mapped. The films have been investigated

Molecular Simulation
ISSN 0892-7022 print/ISSN 1029-0435 online
http://www.tandf.co.uk/journals
DOI: 10.1080/08927020412331332695

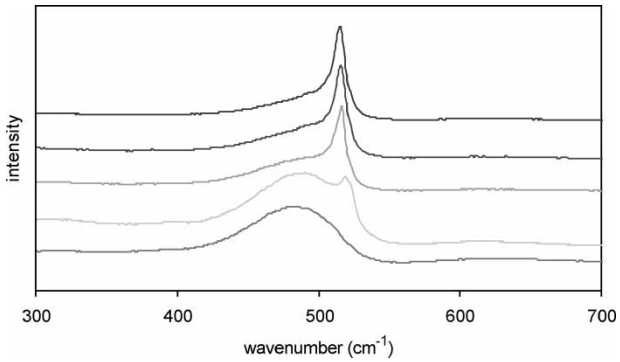

Figure 1. Raman spectra of thin films of silicon deposited by hot wire technique at different filament temperatures, showing the transition from amorphous to microcrystalline. Reading upwards, the lines are for filament temperatures of 1300, 1400, 1500, 1600 and 1700°C, respectively.

using UV–visible spectroscopy, Raman spectroscopy, Fourier transform infra-red spectroscopy, FTIR, transmission electron microscopy, TEM and selected area electron diffraction, SAD.

Anisotropic alkaline etching is widely used in fabrication of industrial silicon solar cells in order to reduce reflection losses from the front surface [5–7]. Selected films were anisotropically etched to enhance the nanocrystalline features and the resulting films have been re-analysed. The etchant consists of 1% NaOH in water with 20% isopropyl alcohol at a temperature of 30°C. Due to the low temperature, a reflux system was not necessary; the substrates were suspended in the solution from a teflon jig. To find the rate of material removal, the thickness of amorphous silicon samples were determined by UV–vis spectroscopy before and after a period of etching. This solution was found to remove the amorphous material at the rate of 1.7 nm per min.

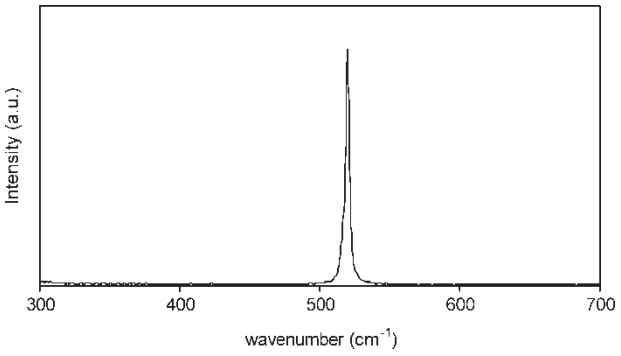

Figure 2. Raman spectrum of a single crystal of silicon.

3. Results

3.1 Crystallinity

The technique of Raman spectroscopy gives clear indications of the onset of crystallinity in amorphous films. Typical Raman Spectra for a range of as-deposited films are shown in figure 1. The spectrum shown in figure 1 is of a film that is completely amorphous, having a single broad peak at 480 cm^{-1}. In contrast, the spectrum in figure 2 is for a single crystal of silicon. In this case the dominant peak is sharp and is centred at 520 cm^{-1}. Figure 1 also shows films with increasing degrees of crystallinity as the filament temperature is increased.

The spectra may be decoupled [8] as shown in figure 3, in which case a third peak becomes evident and in general three peaks are needed to represent the spectrum. The first peak at 480 cm^{-1} is the amorphous component, the third peak at 520 cm^{-1} is the crystalline component. A third, intermediate peak centred at 510 cm^{-1} is generally referred to as arising due to grain boundaries [3].

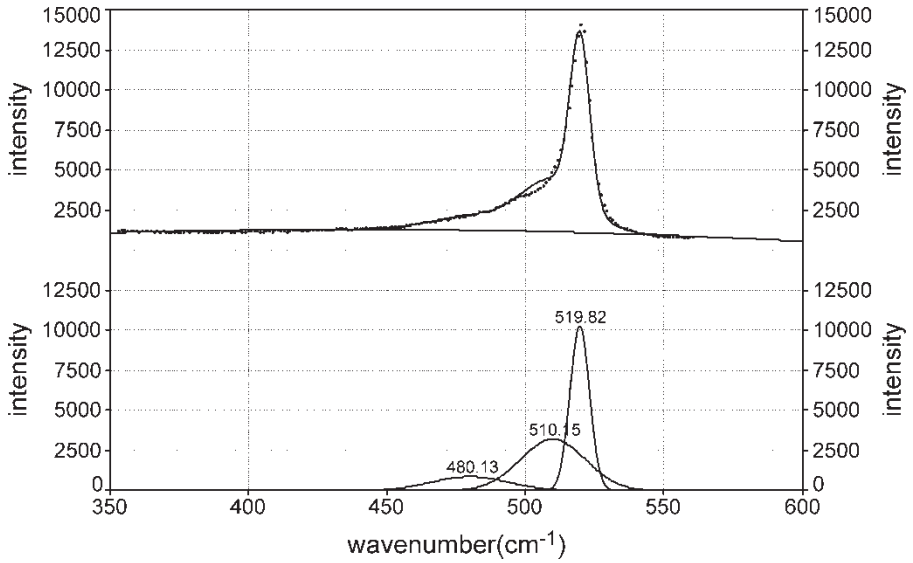

Figure 3. Decoupling using "peakfit" of the Raman spectra obtained at a filament temperature of 1700°C. The amorphous silicon phase has a low intensity; centred at 480 cm^{-1}, with slightly higher intensity for the intermediate; centred at 510 cm^{-1} and the crystalline silicon 520 cm^{-1} phase.

The crystalline volume fraction X_c is calculated from the Raman spectrum as follows:

$$X_c = \frac{(I_c + I_m)}{(I_c + I_m + andsigma; I_a)}$$

Where σ, the ratio of integrated Raman cross section for the amorphous phase to the crystalline phase, is unity, I_c is the integrated intensity of the crystalline peak at $520\,cm^{-1}$, I_m is the integrated intensity of the intermediate phase or grain boundaries between 500 and $510\,cm^{-1}$ and I_a is the integrated intensity of the amorphous peak at $480\,cm^{-1}$ [9,10]. Voids and grain boundaries might contain a high density of recombination centres, whereas a high crystalline fraction is likely to increase the mobility of the charge carriers [11].

Figure 4 shows the variation of crystalline fraction with the two dominant variables of filament temperature and gas flow rate. It can be seen that there is a gradual transition from amorphous to microcrystalline as the filament temperature increases and as the flow rate decreases. Substrate temperature and system pressure were found to have a relatively minor influence on the crystallinity of the samples and will not be shown.

Figure 5 shows the Raman spectra of a film with nano- or protocrystallites. In the as-deposited spectrum, the "$520\,cm^{-1}$" peak is just visible against the broad amorphous peak. It is also shifted from the bulk position. The other lines show how the anisotropic etching has made the crystalline peaks more evident and these have shifted to lower wavenumbers as the nanocrystallites have also been reduced in size by the process. When the crystallites are nanometres in size, the centre frequency of the crystalline peak shifts from the bulk crystal value. It also broadens compared to the crystalline peak. These two features may be used to calculate the size of the nanocrystallites. Figures 6, 7 and 8 show the decoupled peaks for the spectra of figure 5, clearly showing the reduction in amorphous phase and the small reduction in size of the crystallites.

The largest change is in the "grain boundaries" component, this has been reduced substantially. This is not taken into account by the equation conventionally

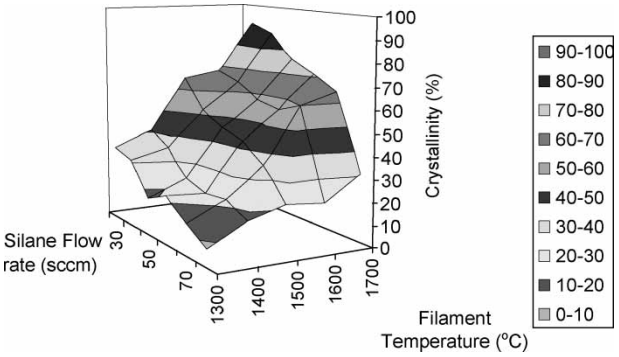

Figure 4. The degree of crystallinity is plotted on the z-axis, with the two dominant variables of filament temperature and silane flow rate plotted on the other two axes. The key shows the % crystallinity of the samples as determined from the Ramam spectra.

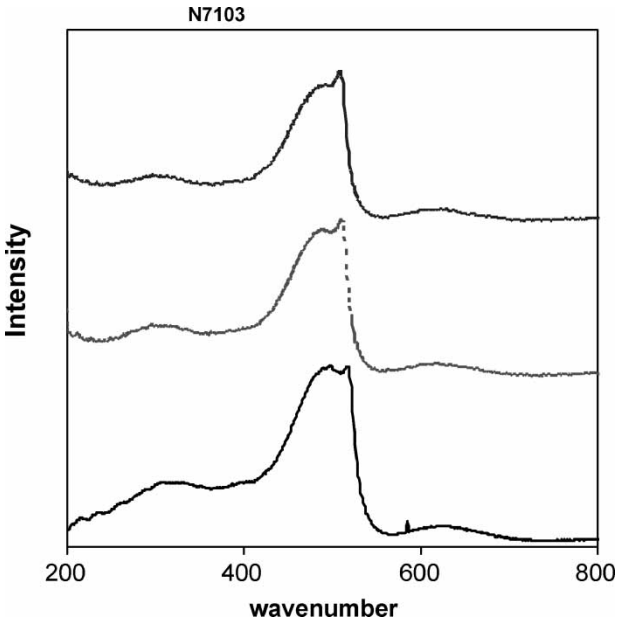

Figure 5. The Raman spectra of a film at the onset of the growth of with nano- or protocrystallites before and after alkaline etching. The lower line is the as-deposited spectrum. The "$520\,cm^{-1}$" peak is just visible against the broad amorphous peak. It is also shifted from the bulk position. The lines above show the same film after periods of anisotropic etching of 3 min and a further 2 min, respectively, which has preferentially removed the amorphous phase. The crystalline peaks are now more evident and have shifted to lower wavenumbers as the nanocrystallites have also been reduced in size by the etch.

used, which indicates little change in X_c. However, inspection of the integrated areas of table 1 clearly show that, whereas the amorphous component diminishes by a factor of three, the crystalline component only reduces by about 20%.

3.2 Hydrogen content

As the film transition progressed from completely amorphous to completely crystalline, the hydrogen content was measured from the FTIR spectra [12] and found to decrease. In the amorphous film, the hydrogen content may be as large as 14% depending on deposition conditions. In microcrystalline material, the hydrogen content may be as low as 1%. At intermediate structures, the hydrogen content also has intermediate values. In the amorphous silicon film, the random structure creates a large number of dangling bonds. Hydrogen atoms are preferentially bonded to these dangling bonds. As the structure becomes more regular, the number of dangling bonds decreases and there are fewer sites for the hydrogen—in a sense the hydrogen is squeezed out of the crystalline structure. Some hydrogen may still be trapped in voids, but as molecular hydrogen and this would not be detected by the FTIR spectroscopy.

3.3 Transition region

There is large Raman signal attributed to grain boundaries, even when there are few small proto or nanocrystallites.

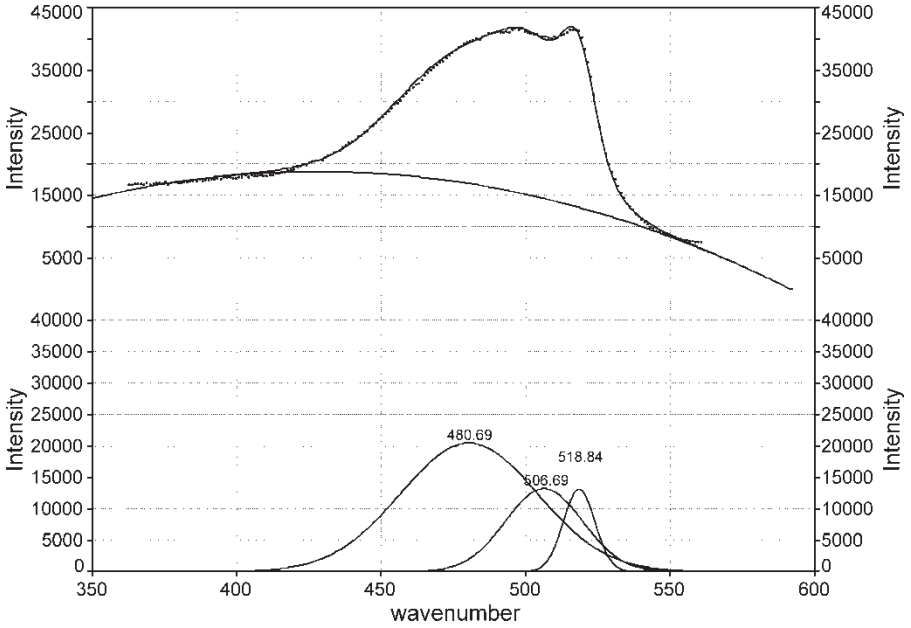

Figure 6. The Raman spectrum for the as-deposited film in Figure 5, showing the decoupled peaks.

We believe that the signal in question arises due to a region around each crystallite, which has a degree of disorder less than the amorphous phase but more than the crystallite [13]. This region gives rise to a distinctly different signal in the Raman spectra, but is not readily differentiated by other investigation techniques. This results in an observed discrepancy, where different techniques appear to give different crystallite sizes [14]. The alkaline etching attacks the three phases to different degrees, hence the changes shown in figures 6, 7 and 8. It can be seen from table 1. that the highly ordered crystallite is affected the least by the etch, and the presence of hydrogen in the amorphous matrix acts to passivate this material and reduce the effect of the etch; hence, the transition material is removed to the greatest degree.

3.4 Electron microscopy

Samples similar to those having Raman spectra as shown in figures 2 and 5 have been viewed in TEM and the results are shown in figures 9, 10 and 11 together with the selected area diffraction pattern in each case. The featureless amorphous film in figure 9 has a selected area diffraction, SAD, pattern showing only broad diffraction rings. The onset of crystallinity seen in figure 10 shows well-defined crystallites in the TEM image and a few

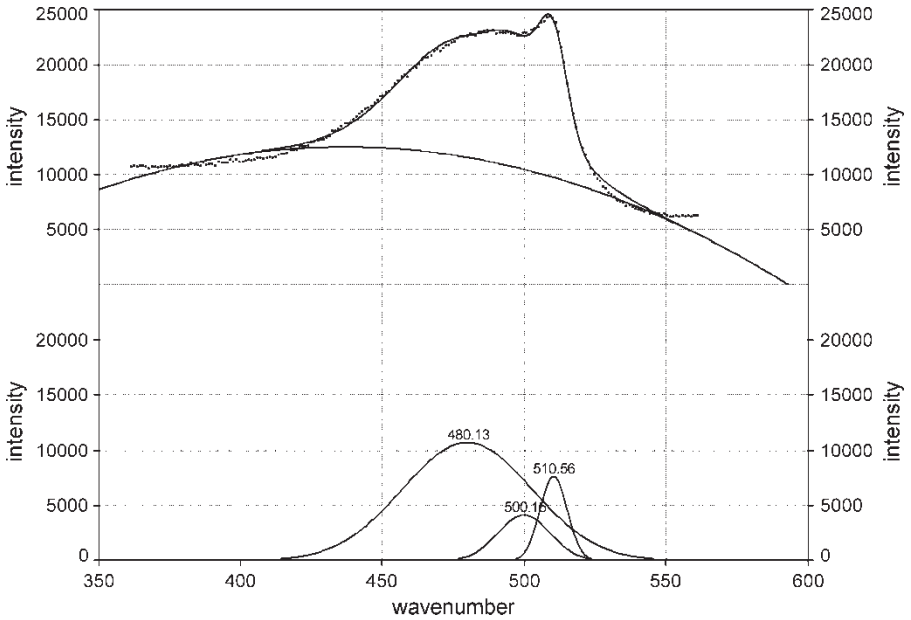

Figure 7. The Raman spectrum for the film in Figure 5 after 3 min of etching, showing the decoupled peaks.

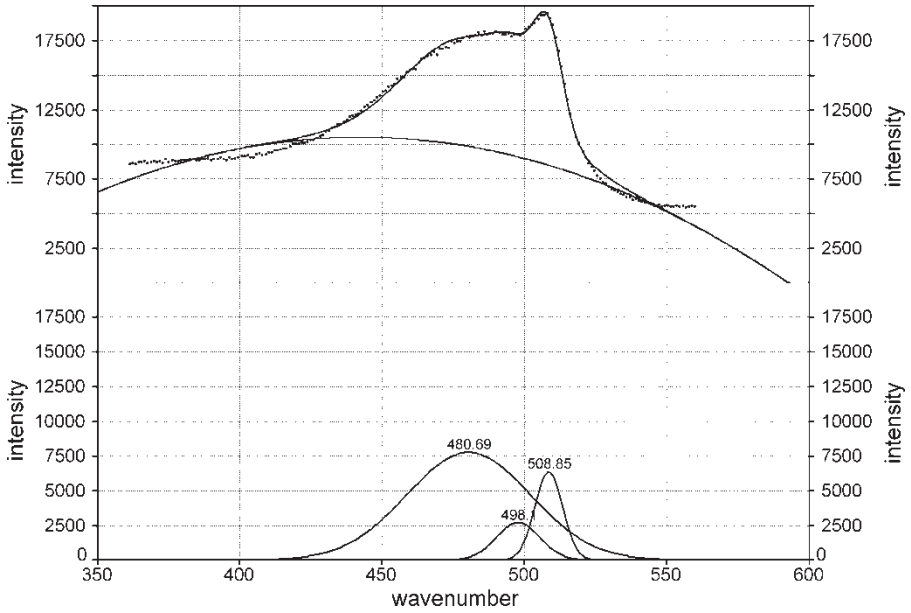

Figure 8. The Raman spectrum for the film in Figure 5 after 5 min of etching, showing the decoupled peaks.

bright diffraction spots in the SAD pattern superimposed on diffuse rings. Figure 11 shows a well-developed crystalline structure and the SAD pattern has bright diffraction spots superimposed on sharper diffraction rings.

4. Conclusion

We have identified the range of parameters for the deposition of nanocrystallites of silicon embedded in an amorphous silicon matrix. We have demonstrated one technique for the enhancement of the crystalline fraction. The alkaline etching appears to work by a combination of removal of the stressed transition layer (intermediate phase) between the true crystal and the amorphous matrix,

Table 1. The integrated areas under the peaks from Figures 6, 7 and 8 have been calculated using the peakfit software. X_c calculated using the equation above is shown for reference.

Film status	I_a	I_m	I_c	X_c
As-deposited	1.216×10^6	0.443×10^6	0.098×10^6	26%
3 min etch	0.612×10^6	0.096×10^6	0.092×10^6	23%
5 min etch	0.423×10^6	0.052×10^6	0.078×10^6	23%

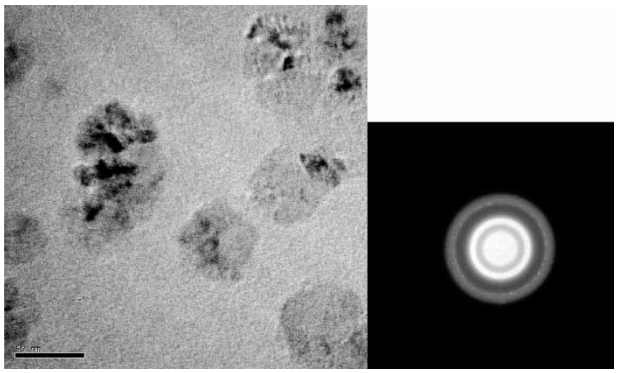

Figure 10. Electron micrograph of crystallites embedded in amorphous silicon thin film matrix and selected area diffraction pattern of same.

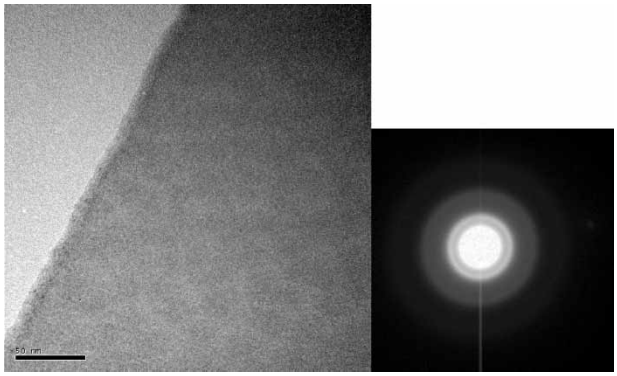

Figure 9. Electron micrograph of amorphous silicon thin film. Its selected area diffraction pattern is shown on the right.

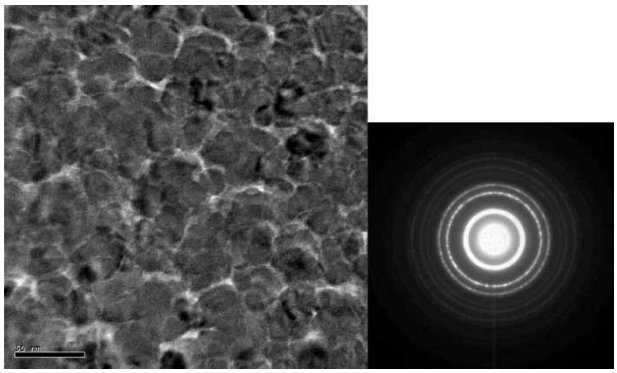

Figure 11. Electron micrograph of almost fully crystalline silicon thin film and selected area diffraction pattern of same.

and reduction in the amorphous matrix itself. The conventional equation for estimating the crystalline fraction has been shown to have limitations.

Acknowledgements

The authors wish to acknowledge the significant contribution of Rob Hart at Curtin University in imaging the samples using electron microscopy techniques and providing training in their use and interpretation and support from the Murdoch University research funding scheme which made this possible.

References

[1] I. Roca, P. Cabarrocas. New approaches for the production of nano-, micro-, and polycrystalline silicon thin films. *Phys. Stat. Sol. (c)*, **1**(5), 1115 (2004).
[2] R.E.I. Shropp, M. Zeman. *Amorphous and Microcrystalline Silicon Solar Cells, Modeling, Materials and Device Technology*, Academic Press, Massachusetts (1998).
[3] A.V. Shah, J. Meier, E. Vallat-Sauvain, N. Wyrsch, U. Kroll, C. Droz, U. Graf. Material and solar cell research in microcrystalline silicon. *Sol. Energy Mat. Sol. Cells*, **78**, 469 (2003).
[4] Mohamed, E., Cornish, J.C.L., Santjojo, D.J., *Rev. Sci. Instrum.*, submitted for publication.
[5] Jandel, peakfit, San Rafael, California, Jandel Scientific Software, 1995.
[6] J. Szlufcik, S. Sivoththaman, J.F. Nijs, R.P. Mertens, R. Van Overstraeten. Low-cost industrial technologies of crystalline silicon solar cells. *Proc. IEEE*, **85**, 711 (1984).
[7] I. Zubel, M. Kramkowska. The effect of isopropyl alcohol on etching rate and roughness of (1 0 0) Si surface etched in KOH and TMAH solutions. *Sens. Actuators A*, **93**, 138 (2001).
[8] E. Vazsonyi, Z. Vertesy, A. Toth, J. Szlufcik. Anisotropic etching of silicon in a two-component alkaline solution. *J. Micromech. Microeng.*, **13**, 165 (2003).
[9] M. Wakagi, T. Kaneko, K. Otat, A. Nakano. *M.R.S. Symp. Proc.*, **283**, 555 (1993).
[10] D. Han, K. Wang, J. Owens, L. Gedvilas, B. Nelson, H. Habuchi, M. Tanaka. Hydrogen structures and the optoelectronic properties in transition films from amorphous to microcrystalline silicon prepared by hot-wire chemical vapor deposition. *J. Appl. Phys.*, **93**, 3776 (2003).
[11] C. Smit, R.A.C. Van Swaaij, H. Donker, A.M.H.N. Petit, W.M.M. Kessels, M.C.M. Van Saden. Determining the material structure of microcrystalline silicon from Raman spectra. *J. Appl. Phys.*, **94**, 3582 (2003).
[12] W. Beyer. *Semiconductors and semimetals*, E.N.H. Nickel (Ed.), Vol. 6, p. 165, Academic Press, San Diego, CA (1999).
[13] J. Kocka, A. Fejfar, T. Mates, P. Fojtik, K. Dohnalova, K. Luterova, J. Stuchlik, H. Stuchlikova, I. Pelant, B.A. Stemmer, M. Ito. The physics and technological aspects of the transition from amorphous to microcrystalline and polycrystalline silicon. *Phys. Stat. Sol., (c)*, 1097 (2004).
[14] O. Vetterl, F. Finger, R. Carius, P. Hapke, L. Houben, O. Kluth, A. Lambertz, A. Muck, B. Rech, H. Wagner. Thickness dependence of microcrystalline silicon solar cell properties. *Sol. Energy Mat. Sol. Cells*, **62**, 97 (2000).